1984

A finite element analysis of a creeping beryllium plate /

Gary L. Povirk
Lehigh University

A FINITE ELEMENT ANALYSIS OF A CREEPING BERYLLIUM PLATE

by

Gary L. Povirk

A Thesis

Presented to the Graduate Committee

of Lehigh University

in Candidacy for the Degree of

Master of Science

in

Mechanical Engineering

Lehigh University

1984

This thesis is accepted and approved in partial fulfillment of the requirements for the degree of Master of Science.

Dec 16, 1954

(date)

Jerry J. Delgado

Professor in Charge

F. Erdogan

Chairman of Department

ACKNOWLEDGEMENTS

The author wishes to express his sincere appreciation to Professor Terry J. Delph for his invaluable guidance and patience during the preparation of this thesis.

TABLE OF CONTENTS

ABSTRACT

The creep of a centrally loaded, simply supported beryllium plate is predicted by the use of a finite element code. A creep constitutive law based upon creep data obtained from the National Bureau of Standards (NBS) was utilized in the code. Two sets of curve fits were done because of a wide divergence in data at the same stress level. The resulting uniaxial constitutive laws are written in strain hardening form, and are generalized into multiaxial creep laws. The finite element code's predictions after 10,000 hours are compared with the results of a test performed at NBS. Comparisions show that one fit provides a good estimate of the plate deflection, while the other does not. It is felt that differences in predictions can be attributed to the large discrepancies in the data and not to the finite element code itself.

INTRODUCTION

Beryllium is a metal often used in gyroscope components in inertial guidance systems because of its superior specific strength. A problem with beryllium, however, is that it exhibits microcreep- that is, it creeps very slightly even at room temperature and fairly low stresses. Because current design practice specify that the movement of the center of mass of the gyroscope be less than 25 ρm, a means of predicting the creep of the components would be useful [1]. To do this, a creep constitutive law valid under multiaxial stress states must be developed for beryllium.

Typically, a multiaxial creep law is determined by first conducting uniaxial tests at several different levels of stress. A uniaxial creep law can be fitted to the experimental data, usually of the form:

$$\varepsilon^c = f(\sigma,t) \tag{1.1}$$

This can be differentiated with respect to time to give the so called time hardening creep formulation:

$$\dot{\varepsilon}^c = \frac{\partial}{\partial t} g(\sigma,t) \tag{1.2}$$

However, often t can be determined in terms of σ and ε^c from equation (1.1) and this result can be substituted into equation (1.2) to give what is called the strain hardening creep formulation [2].

$$\dot{\varepsilon}^c = g(\sigma, \varepsilon^c) \qquad (1.3)$$

Because tests with varying states of stress have shown that the strain hardening formulation is more accurate [2], it will be used in this investigation. Other experimental and theoretical considerations show that the following should hold true for a multiaxial creep law:

(1) the multiaxial law should reduce to the uniaxial creep law under uniaxial stress conditons.

(2) For isotropic materials, the principal stress and strain axes should coincide.

(3) Experimental evidence suggests that the inelastic strains are incompressible, i.e., $\varepsilon^c_{kk}=0$, so that there is no dependence upon the hydrostatic stress $P=1/3\sigma_{kk}$. Thus only the deviatoric stress $S_{ij}= \sigma_{ij} - 1/3\ \sigma_{kk}\delta_{ij}$ influences the inelastic strain.

From these considerations, a possible form of the multiaxial creep law is:

$$\dot{\varepsilon}^c_{ij} = h(\bar{\sigma}, \bar{\varepsilon}^c)S_{ij} \qquad (1.4)$$

where $\bar{\sigma}$ and $\bar{\varepsilon}^c$ are the von Mises stresses and inelastic strains respectively. The intent of this study is to develop such a law,

and implement it into a finite element code. The predictions of the code will be compared with the results from actual tests.

In particular, we will model an experiment carried out on a simply supported, centrally loaded, circular beryllium plate at the National Bureau of Standards in Gaithersburg, Maryland. The circular plate configuration was chosen for several reasons, the principal one being that it represents a simple test which nevertheless yields a spatially varying multiaxial stress state throughout the plate. Also, laser inferometry can measure the deflection of the polished circular plate with very high accuracy ($\pm 10^{-8}$ m). In a typical test, a dead weight loading was applied at the center of the plate and the deflected shape was measured periodically up to a time of 10,000 hours.

In order to implement the creep law into a finite element program, the equilibrium equation for a circular plate as derived by Timoshenko and Woinowsky-Krieger [3] was modified to include the tangential and radial creep strains. Use of the Galerkin method yields the finite element equations used in the program. Then the equations are integrated through time to 10,000 hours by the Adams-Bashforth predictor-corrector integration scheme [4]. Since the finite element method can easily be applied to odd shaped bodies, the results learned here should be readily transferable to inertial guidance components.

DEVELOPMENT OF MULTIAXIAL CREEP LAW FOR BERYLLIUM

From the National Bureau of Standards (NBS), three sets of uniaxial creep data for beryllium were obtained, one at 20.7 MPa and two others at 69.0 MPa (see Figure 1). Because of material science considerations [5], the creep strains are chosen to be a function of σ and t in the form:

$$\varepsilon^c = A(\sigma)\ln(1+t/B(\sigma)) \qquad (2.1)$$

Standard curve fitting techniques applied at NBS yielded the following values of A and B for the 20.7 MPa test and the 69.0 MPa test that exhibited smaller strains.

Table 1

σ (MPa)	A (μm/m)	B (hours)
20.7	.110	1.21
69.0	.162	.069

Because the secondary or steady state creep rate is often a power law function of stress, the function $A(\sigma)$ was assumed to take the form:

$$A(\sigma) = A_0\sigma^n \qquad (2.2)$$

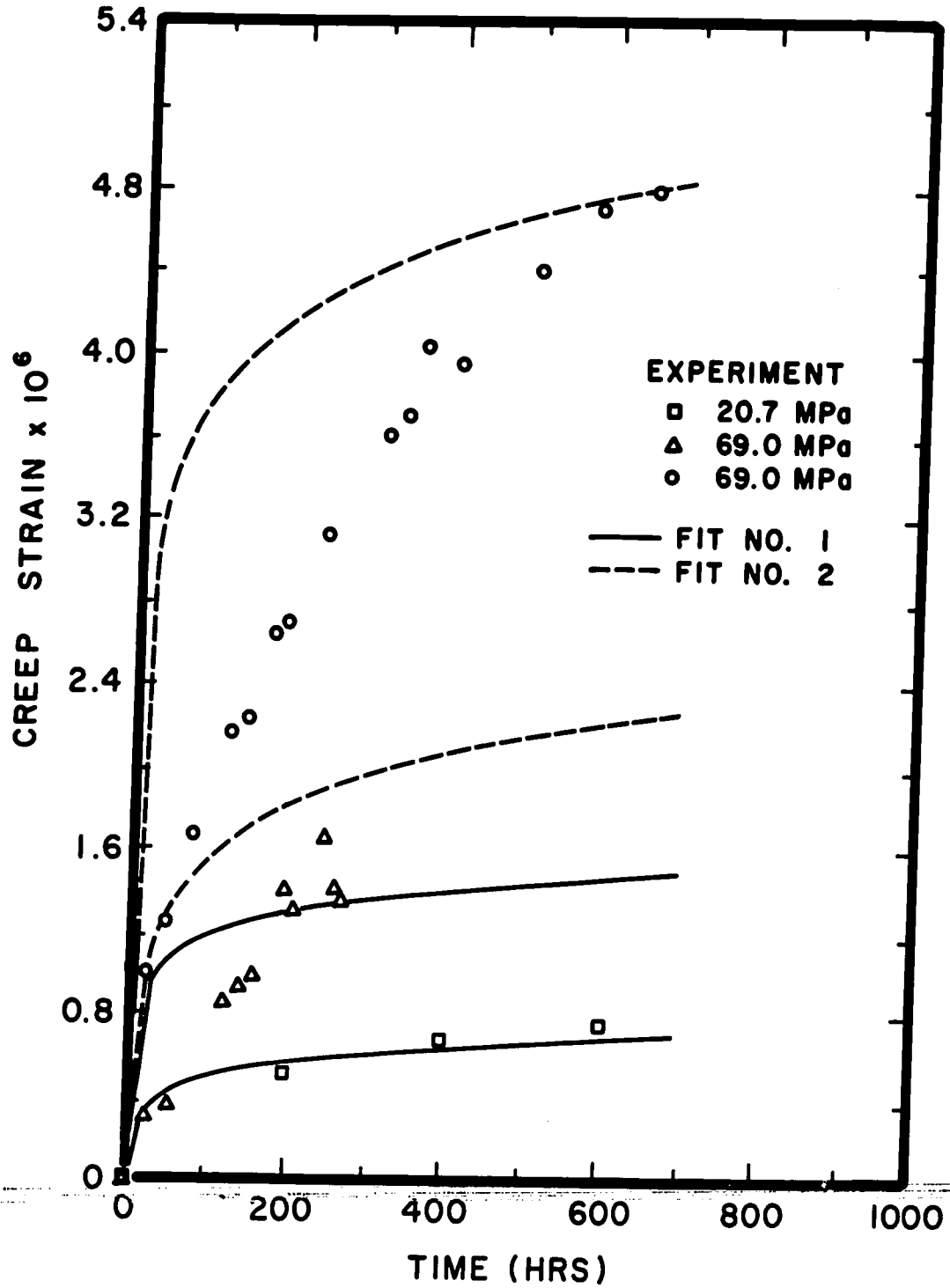
5.4
4.8
4.0
3.2
2.4
1.6
0.8
0
CREEP STRAIN x 10⁶
0
200
400
600
800
1000
TIME (HRS)
EXPERIMENT
20.7 MPa
69.0 MPa
69.0 MPa
FIT NO. 1
FIT NO. 2

Fig. 1.

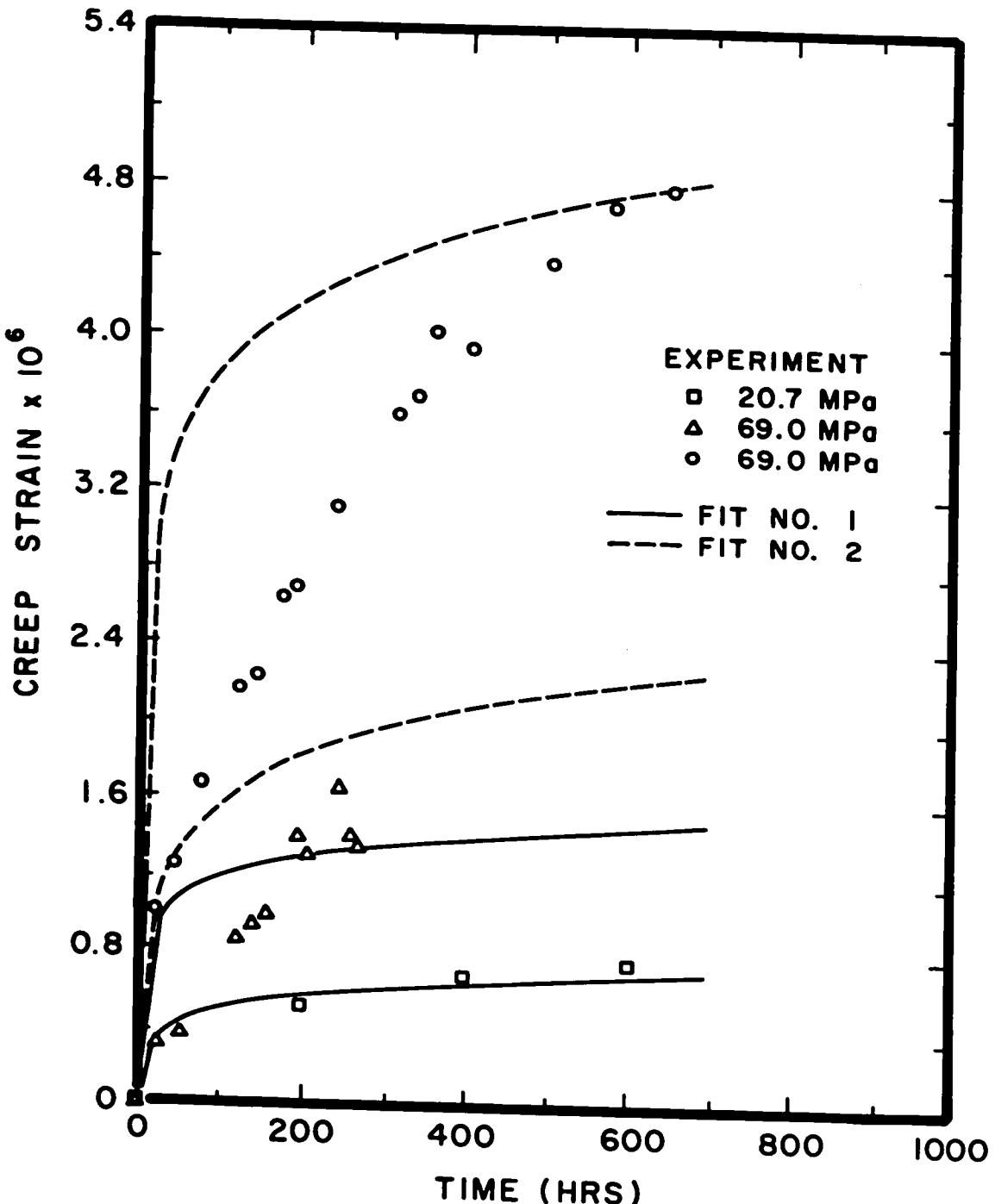
5.4
4.8
4.0
3.2
2.4
1.6
0.8
0
CREEP STRAIN x 10^6
0
200
400
600
800
1000
TIME (HRS)
EXPERIMENT
20.7 MPa
69.0 MPa
69.0 MPa
FIT NO. 1
FIT NO. 2

Fig. 1.

$B(\sigma)$ was arbitrarily chosen to be a linear function of σ so that $B(\sigma)$ can be written:

$$B(\sigma)=B_0+B_1\sigma \qquad (2.3)$$

so that equation (2.1) now reads:

$$\varepsilon^c=A_0\sigma^n\ln(1+t/(B_0+B_1\sigma)) \qquad (2.4)$$

Fitting the assumed functions $A(\sigma)$ and $B(\sigma)$ for the values given in Table 1 gives the following values for n, A_0^1, B_0 and B_1.

$n=.322$

$A_0^1=4.15\text{x}10^{-8}$ $(\text{MPa})^{-n}$

$B_0=-.0236$ (hours)

$B_1=1.70$ (hours/MPa)

These values were inserted into equation (2.4) to obtain creep law #1 shown in Figure 1. However, because of the substantial differences between the results of the two tests conducted at 69.0 MPa, it was felt that another set of fits were required in order to understand how the discrepancies between the two 69.0 MPa tests might affect the result of the finite element analysis. This was accomplished by leaving n, B_0, and B_1 the same as before, reading off the inelastic strain from the higher set of creep data at 69.0

MPa and at t equal to about 650 hours, and solving for A_0^*. In this way, A_0^* was found to be:

$$A_0^* = 1.37 \times 10^{-7} \ (\text{MPa})^{-n}$$

While both the creep laws obtained do not fit the experimental data particularily well during the first few hundred hours, comparisions between the actual and predicted plate deflections occured at t=10,000 hours, and therefore short term inaccuracies can be discounted.

At this point, the uniaxial creep law has to be put in the strain hardening form $\dot{\varepsilon}^c = g(\sigma, t)$ mentioned in the Introduction. Differentiating equation (2.1) with respect to time while holding the stress constant gives:

$$\dot{\varepsilon}^c = \frac{A(\sigma)}{(1+t/B(\sigma))} \cdot \frac{1}{B(\sigma)} = \frac{A(\sigma)}{B(\sigma)+t} \qquad (2.5)$$

Solving for t from equation (2.1) yields:

$$t = B(\sigma)\varepsilon\exp(\varepsilon^c/A(\sigma)) - B(\sigma) \qquad (2.6)$$

Substitution back into equation (2.5) gives:

$$\dot{\varepsilon}^c = \frac{A_0 \sigma^n}{B_0 + B_1 \sigma} \exp(-\varepsilon^c / A_0 \sigma^n) \qquad (2.7)$$

Now the uniaxial creep law can be generalized into a multiaxial law. To do this, it will be assumed that the total strain rate can be written as the sum of the elastic and inelastic strain rates:

$$\dot{\varepsilon}_{ij} = \dot{\varepsilon}^E_{ij} + \dot{\varepsilon}^c_{ij} \qquad (2.8)$$

where the elastic strain rate, $\dot{\varepsilon}^E_{ij}$ can be found by Hooke's law. Notice that the second and third considerations given in the Introducton can be satisfied by writing:

$$\dot{\varepsilon}^c_{ij} = \lambda(S_{ij}, \varepsilon^c_{ij})\, S_{ij} \qquad (2.9)$$

where S_{ij} is the deviatoric stress tensor and $\lambda(S_{ij}, \varepsilon_{ij})$ is a scalar function of the stress deviator and the inelastic strain tensor. Because the stress deviator is defined as:

$$S_{ij} = \sigma_{ij} - \sigma_{kk}/3 \qquad (2.10)$$

it effectively removes any dependence of hydrostatic stress on the creep law. Also note that the inelastic strains are incompressible:

$$\dot{\varepsilon}^c_{kk} = \lambda(S_{11} + S_{22} + S_{33}) = 0 \qquad (2.11)$$

and that the principal axes of stress and strain coincide.

$$\dot{\varepsilon}^c_{ij} = \lambda S_{ij} \tag{2.12}$$

However, if λ is to be invariant under coordinate rotations, then it must depend only on the invariants of the deviatoric stress and inelastic strain tensors. For a 3x3 symmetric tensor b_{ij}, the invariants are given by:

$$\begin{aligned} I_b &= b_{ii} \\ II_b &= b_{ij}b_{ij} \\ III_b &= b_{ij}b_{jk}b_{ki} \end{aligned} \tag{2.13}$$

Because $I_s = S_{kk} = 0$ and $I_{\varepsilon}c = \varepsilon^c_{kk} = 0$, the dependence can only be on the second and third invariants. Typically, however, and with some experimental support, λ is taken to depend only on the second invariants of S_{ij} and ε_{ij}. A convenient way to express this dependence is through the von Mises stress and strain quantities $\bar{\sigma}$ and $\bar{\varepsilon}$, where:

$$\bar{\sigma} = (3/2\ II_s)^{1/2} = (3/2\ S_{ij}S_{ij})^{1/2} \tag{2.14}$$

$$\bar{\varepsilon}^c = (2/3\ II_{\varepsilon}c)^{1/2} = (2/3\ \varepsilon^c_{ij}\varepsilon^c_{ij})^{1/2} \tag{2.15}$$

The inelastic strain rate can therefore be written:

$$\dot{\varepsilon}^c_{ij} = \lambda(\bar{\sigma},\bar{\varepsilon}^c)S_{ij} \qquad (2.16)$$

Notice that for the case of uniaxial tension along the x_1 axis, for example, the von Mises stresses and strains reduce to $\bar{\sigma}=\sigma_{11}$ and $\bar{\varepsilon}=\varepsilon_{11}$. The function $\lambda(\bar{\sigma},\bar{\varepsilon}^c)$ can be found by insisting that it reduce to the uniaxial form (equation (2.8)) under uniaxial conditions. Thus $\dot{\varepsilon}^c_{11}$ is equal to:

$$\dot{\varepsilon}^c_{11} = \lambda(s_{11},\varepsilon^c_{11})\ \frac{2\sigma_{11}}{3} = \frac{A_0\sigma_{11}^n}{B_0 + B_1\sigma_{11}} \exp(-\varepsilon_{11}/A_0\sigma_{11}^n) \qquad (2.17)$$

Solving for $\lambda(\sigma_{11},\varepsilon_{11})$ gives:

$$\lambda(\sigma_{11},\varepsilon^c_{11}) = 3/2\ \frac{A_0\sigma_{11}^{n-1}}{B_0 + B_1\sigma_{11}} \exp(-\varepsilon^c_{11}/A_0\sigma_{11}^n) \qquad (2.18)$$

In this way, the multiaxial creep law for beryllium takes the form:

$$\dot{\varepsilon}^c_{ij} = 3/2\ \frac{A_0\bar{\sigma}^{n-1}}{B_0 + B_1\bar{\sigma}} \exp(-\bar{\varepsilon}^c/A_0\bar{\sigma}^n)S_{ij} \qquad (2.19)$$

It is this multiaxial creep law that will be inserted into a finite element code to predict the deflection of the plate as a function of time.

IMPLEMENTION OF THE MULTIAXIAL CREEP LAW INTO A FINITE ELEMENT CODE

In order to characterize the effects of creep in a circular beryllium plate, a few basic relations are needed. The following kinematic and equilibrium equations were obtained from Timoshenko and Woinowsky-Krieger [3]:

$$\varepsilon_r = -z\frac{d^2w}{dr^2} \tag{3.1}$$

$$\varepsilon_t = \frac{-z}{r}\frac{dw}{dr} \tag{3.2}$$

$$M_r + r\frac{dM}{dr}r - M_t + Qr = 0 \tag{3.3}$$

where w is the deflection of the plate, M_r and M_t are the moments per unit length in the radial and tangential directions respectively, and Q is the shearing force per unit length (See Figure 2 for sign conventions). The objective of the following derivation will be to write the equilibrium equation as a time dependent partial differential equation governing the deflection (or the slope) of the plate, and including the radial and tangential creep strains.

The moments M_r and M_t can be found by multiplying the radial or tangential stress by the moment arm z, and integrating through the thickness of the plate. Thus:

$$M_r = \int_{-h/2}^{h/2} \sigma_r z \, dz \tag{3.4}$$

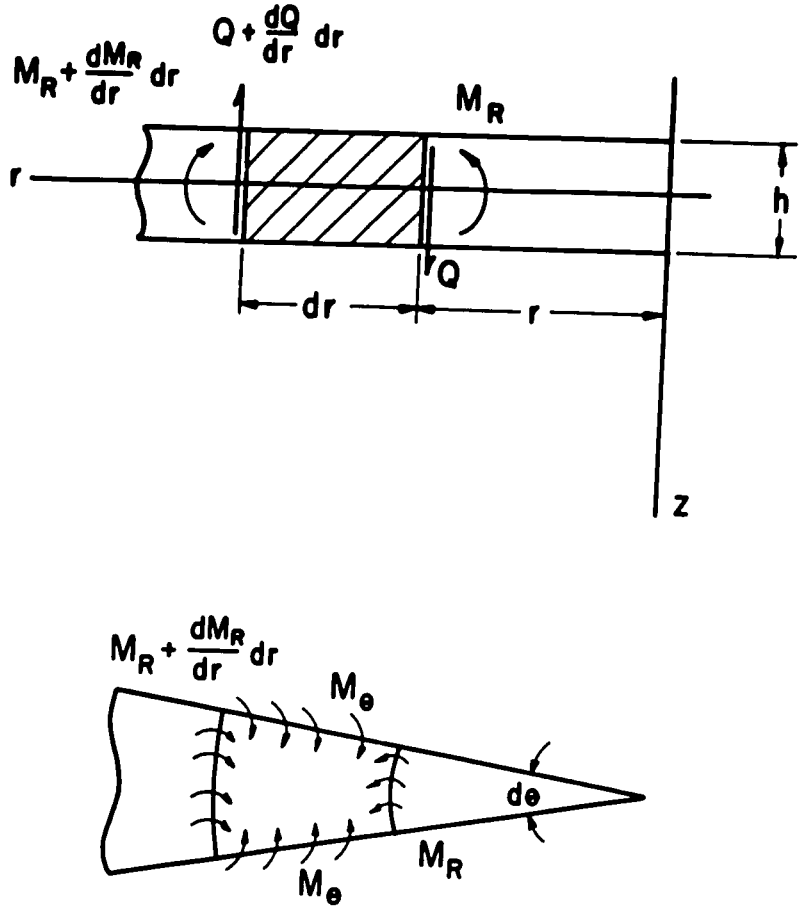
$Q + \frac{dQ}{dr} dr$
$M_R + \frac{dM_R}{dr} dr$
M_R
r
h
Q
dr
r
z
$M_R + \frac{dM_R}{dr} dr$
M_θ
$d\theta$
M_R
M_θ

Fig. 2.

$$M_t = \int_{-h/2}^{h/2} \sigma_t z \, dz \tag{3.5}$$

The radial and tangential creep strains can be found in terms of the elastic and total strains by simply subtracting the elastic strain from the total strain.

$$\varepsilon_r^c = \varepsilon_r - \varepsilon_r \tag{3.6}$$

$$\varepsilon_t^c = \varepsilon_t - \varepsilon_t \tag{3.7}$$

Also, since a thin circular plate is a plane stress problem, Hooke's Law takes the following form:

$$\sigma_r = \frac{E}{1-v^2} (\varepsilon_r + v\varepsilon_t) \tag{3.8}$$

$$\sigma_t = \frac{E}{1-v^2} (v\varepsilon_r + \varepsilon_t) \tag{3.9}$$

where E is Young's Modulus and v is Poisson's ratio. Combining equations (3.1),(3.2),(3.6) and (3.7) with Hooke's Law yields:

$$\sigma_r = \frac{E}{1-v^2}\left[z\frac{\partial^2 w}{\partial r^2} - \varepsilon_r^c + v\frac{z}{r}\frac{\partial w}{\partial r} - v\varepsilon_t^c \right] \tag{3.10}$$

$$\sigma_t = \frac{E}{1-v^2}\left[\frac{z}{r}\frac{\partial w}{\partial r} + \varepsilon_t^c + vz\frac{\partial^2 w}{\partial r^2} - v\varepsilon_r^c \right] \tag{3.11}$$

Substituting the above equations for σ_r and σ_t into equations (3.4) and (3.5) gives:

$$M_r = D\left[\frac{\partial^2 w}{\partial r^2} + \frac{\nu}{r}\frac{\partial w}{\partial r} \right] - \frac{E}{1-\nu^2}\int_{-h/2}^{h/2} z(\varepsilon_r^c + \nu\varepsilon_t^c)\,dz \qquad (3.12)$$

$$M_t = D\left[\frac{1}{r}\frac{\partial w}{\partial r} + \nu\frac{\partial^2 w}{\partial r^2} \right] - \frac{E}{1-\nu^2}\int_{-h/2}^{h/2} z(\varepsilon_t^c + \nu\varepsilon_r^c)\,dz \qquad (3.13)$$

where $D = \frac{Eh^3}{12(1-\nu^2)}$ and h is the plate thickness. Also, for a circular plate with a centrally applied point load, the transverse shear force per unit length, Q, can be written as:

$$Q = \frac{P}{2\pi r} \qquad (3.14)$$

Substitution of the expressions for M_r, M_t and Q (equations (3.12), (3.13) and (3.14)) into the equilibrium equation (3.3) results in a partial diferential equation governing the deflection, w, and containing the creep strains.

$$r\frac{\partial^3 w}{\partial r^3} + \frac{\partial^2 w}{\partial r^2} - \frac{1}{r}\frac{\partial w}{\partial r} = \frac{E}{D(1-\nu^2)}\int_{-h/2}^{h/2}\frac{\partial}{\partial r}(\varepsilon_r^c + \nu\varepsilon_t^c)\,dz$$

$$+ \frac{E}{D(1+\nu)}\int_{-h/2}^{h/2}(\varepsilon_r^c - \varepsilon_t^c)\,dz - \frac{P}{2\pi D} \qquad (3.15)$$

The above equation can be made slightly more tractable by a few changes in variables. First, the z integration can be simplified by using a normalized variable ξ, where:

$$\xi = 2z/h \tag{3.16}$$

and by noting that the integrands are symmetric about z=0. Also the radius can be non-dimensionalized by letting:

$$\rho = r/R \tag{3.17}$$

where R is the plate radius. Finally the order of the expression can be reduced by introducing a new variable φ, where φ is defined as $\frac{\partial w}{\partial \rho}$. With these changes, the equilibrium equation now appears as the following:

$$\rho\frac{\partial^2\varphi}{\partial\rho^2} + \frac{\partial\varphi}{\partial\rho} - \frac{\varphi}{\rho} = \frac{Eh^2R^2}{2D(1-\nu^2)}\Big[\,\rho\int_0^1 \xi\,\frac{\partial}{\partial\rho}(\varepsilon_r^c + \nu\varepsilon_t^c)\,d\xi$$

$$+ (1-\nu)\int_0^1 \xi(\varepsilon_r^c - \varepsilon_t^c)\,d\xi\Big] - \frac{PR^2}{2\pi D} \tag{3.18}$$

Obtaining the initial and boundary conditions for the above equation is fairly straightfoward. One boundary condition is that at the center of the plate (ρ=0), the slope, φ, should be zero. The other is that at the edge of the plate (ρ=1), the radial bending moment, M_r, should be zero, since the plate is simply supported. These two conditions and equation (3.12) yield two boundary equations:

$$\varphi(0,t) = 0 \tag{3.19}$$

$$\left[\frac{\partial \phi}{\partial \rho} + \nu \phi\right]_{\rho=1} = \frac{Eh^2R^2}{2D(1-\nu^2)}\int_0^1 \xi(\varepsilon_r^c + \nu\varepsilon_t^c)_{\rho=1}\,d\xi \qquad (3.20)$$

The initial condition is simply that at t=0,

$$\varepsilon_r^c(\rho,\xi,0) = \varepsilon_t^c(\rho,\xi,0) = 0 \qquad (3.21)$$

As stated before, a finite element formulation will be sought for equation (3.18) with the above initial and boundary conditions. By using Galerkin's method [6], equation (3.18) can be rewritten to take the form:

$$\int_0^1 (\rho\frac{\partial^2\phi}{\partial\rho^2} + \frac{\partial\phi}{\partial\rho} - \frac{\phi}{\rho})N_i(\rho)\,d\rho = \frac{Eh^2R^2}{2D(1-\nu^2)}\Big[\int_0^1 \rho N_i(\rho)\int_0^1 \xi\frac{\partial}{\partial\rho}(\varepsilon_r^c+\nu\varepsilon_t^c)\,d\xi\,d\rho$$

$$+ (1-\nu)\int_0^1 N_i(\rho)\int_0^1 \xi(\varepsilon_r^c-\varepsilon_t^c)\,d\xi\,d\rho\Big]$$

$$- \frac{PR^2}{2\pi D}\int_0^1 N_i(\rho)\,d\rho \qquad (3.22)$$

where $N_i(\rho)$ are the interpolating functions. Although C^0 continuous interpolating functions could be used here, C^1 hermitian functions (See Appendix) were chosen because they are relatively simple to implement in the one dimensional case and because they are more accurate than C^0 functions.

Because hermitian interpolating functions interpolate to both ϕ

and $\frac{\partial \phi}{\partial \rho}$ at each nodal point, 2n equations will be obtained for a problem with n nodal points. For convenience, the index i for the interpolating functions $N_i(\rho)$ will be taken to run from 0 to (2n-1). In the indexing system utilized in the Appendix, the interpolating functions corresponding to the even indices 0,2,4... interpolate to the values of ϕ at the n nodal points, while the odd indices 1,3,5... interpolate to the values of $\frac{\partial \phi}{\partial \rho}$. The left hand side of equation (3.22) is now integrated by parts to give:

$$\rho N_i(\rho)\frac{\partial \phi}{\partial \rho}\Big]_0^1 + \int_0^1 (-\rho \frac{\partial N_i(\rho)}{\partial \rho}\frac{\partial \phi}{\partial \rho} - \frac{1}{\rho} N_i(\rho)\ )d\rho \qquad (3.23)$$

From the boundary condition given by equation (3.12), the value of ϕ is known at $\rho=0$. Hence there will be no equation corresponding to i=0 and the index i will run from 1 to (2n-1). Moreover, the first term in equation (3.21) vanishes at the lower limit. At the upper limit of $\rho=1$, the only non zero contribution comes in the (2n-2)th equation where $N_{2n-2}(\rho=1)=1$. Introducing the boundary condition from equation (3.18), this becomes:

$$\frac{\partial \phi}{\partial \rho}\Big]_1 = -v\phi\Big]_1 + \frac{Eh^2R^2}{2D(1-v^2)}\int_0^1 \xi(\varepsilon_r^c + v\varepsilon_t^c)_{\rho=1}d\xi \qquad (3.24)$$

Now ϕ is aproximated by $\phi \cong \sum_{i=1}^{2n-1} N_i(\rho)\Theta_i$ where Θ_i are ϕ or $\frac{\partial \phi}{\partial \rho}$ at each nodal point. For hermitian interpolating functions, then,

becomes:

$$\phi = N_1\phi_0 + N_2\phi_1 + N_3\phi_1 + N_4\phi_2 + N_5\phi_2 + \ldots$$
$$+N_{2n-2}\phi_n + N_{2n-1}\phi'_n \qquad (3.25)$$

where $\phi' = \frac{\partial\phi}{\partial\rho}$ and n is the number of nodal points. Note that ϕ can also be written as a matrix multiplication $[N]\{\Theta\}$ where $[N]$ is a $1x(2n-1)$ matrix of interpolating functions and $\{\Theta\}$ is a $(2n-1)x1$ vector of nodal point values. Substituting $[N]\{\Theta\}$ for ϕ, the integral expression in (3.23) becomes:

$$\int_0^1 (-\rho\frac{\partial N}{\partial\rho}i\ \frac{\partial\phi}{\partial\rho} - N_i\ \frac{\phi}{\rho})d\rho = -\int_0^1 (\rho\frac{\partial N}{\partial\rho}i\left[\frac{\partial N}{\partial\rho}\right] + \frac{N}{\rho}i[N])d\rho\{\Theta\} \qquad (3.26)$$

Additionally, the boundary term in expression (3.23) as it appears in the (2n-2)th equation is:

$$\phi'_{n-1} = -v\phi_{n-1} + \frac{Eh^2R^2}{2D(1-v^2)}\int_0^1 \xi[\varepsilon_r^c + v\varepsilon_t^c]_{\rho=1}d\xi \qquad (3.27)$$

Nine nodal point were thought to be enough for sufficient accuracy. Because the exact elastic solution for this problem is available in closed form, the finite element solution at t=0 can be compared with the exact solution to determine if enough points were used. The nodal points were chosen at ρ =0.0, 0.025, 0.050, 0.10, 0.20, 0.40, 0.60, 0.80, and 1.0 . The points are closer near the

center of the plate because the gradient of the solution can be expected to be greater there. Equation (3.22) can now be written:

$$[K]\{\Theta\} = \{R\} \tag{3.28}$$

where [K] is a 17x17 matrix and

$$K_{ij} = \int_0^1 (\rho \frac{\partial N_i}{\partial \rho} \frac{\partial N_j}{\partial \rho} + \frac{1}{\rho} N_i N_j) d\rho \tag{3.29}$$

From equation (3.24), the boundary term adds v to the matrix element $K_{16,16}$.

$\{\Theta\}$ is a 17x1 vector of the form:

$$\{\Theta\} = \begin{Bmatrix} \phi_0' \\ \phi_1 \\ \phi_1' \\ \phi_2 \\ \phi_2' \\ \cdot \\ \cdot \\ \cdot \\ \phi_8 \\ \phi_8' \end{Bmatrix}$$

and {R} is a 17x1 vector where:

$$R_i = \frac{Eh^2R^2}{2D(1-\nu^2)} \left[\int_0^1 \rho N_i(\rho) \int_0^1 \xi \frac{\partial}{\partial \rho} (\varepsilon_r^c + \nu \varepsilon_t^c) d\xi d\rho \right.$$

$$\left. + (1-\nu) \int_0^1 N_i(\rho) \int_0^1 \xi (\varepsilon - \varepsilon_t^c) d\xi d\rho \right] - \frac{PR^2}{2\pi D} \int_0^1 N_i(\rho) d\rho \tag{3.30}$$

The boundary term (second term on the right hand side of equation (3.27)) is added to the 16th equation to complete the system of equations.

Now that the finite element equations have been fully developed, the coefficients in the equations must be calculated and the equations solved by use of a computer code. The integrals are evaluated by using three point Gaussian integration across each element in the radial direction, and four point integration through the plate thickness [4]. Thus, the stiffness matrix is obtained by first evaluating the interpolating functions and their derivatives at each radial gauss point, integrating equation (3.29) across an element to form an element coefficient matrix, and finally assembling the element matrices into the global stiffness matrix. The matrix is then augmented with the boundary condition at $\rho=1$, and LDL^T decomposed [4]. Since the matrix is constant with time, it needs to be assembled and decomposed only once. In the right hand side vector, the term $\frac{PR^2}{2\pi D}\int_0^1 N_i(\rho)d\rho$ is integrated in a similar manner. The initial nodal point values are then obtained by foward/back substitution[4].

Using equations (3.10) and (3.11) and the initial conditions obtained from the elastic solution, the stresses are calculated at every gauss point and stored in an array. Then, using the multiaxial creep law developed previously, the inelastic strain rates are calculated at each point and are also stored in an array. At this point the rates are integrated through time to give the inelastic strain at $t=\Delta t$. Once the inelastic strains are known

throughout the plate, the gradient of the sum $(\varepsilon_r^c + \nu\varepsilon_t^c)$ is approximated by the use of natural cubic splines (the second derivatives were assumed to be zero at the end points)[4]. In this way, the term $\frac{\partial}{\partial\rho}(\varepsilon_r^c + \nu\varepsilon_t^c)$ is estimated at every gauss point. Because the inelastic strains and strain gradients are now known through out the plate, the integrals

$$\int_0^1 N_i(\rho)\int_0^1 \xi(\varepsilon_r^c - \varepsilon_t^c)d\xi d\rho \quad \text{and}$$

$$\int_0^1 \rho N_i(\rho)\int_0^1 \xi\frac{\partial}{\partial\rho}(\varepsilon_r^c + \nu\varepsilon_t^c)d\xi d\rho$$

can be evaluated by gaussian integration as before, and added to the elastic right hand side vector. However, the inelastic boundary condition, (the integral term in equation (3.27)) must be evaluated and added to the next to last element in the right hand side vector. Because the inelastic strains are not explicitly calculated at $\rho=1$, they are approximated by a first order finite difference equation:

$$\left[\varepsilon_r^c + \nu\varepsilon_t^c\right]_{\rho=1} = \left[\varepsilon_r^c + \nu\varepsilon_t^c\right]_{\rho=\rho^*} + \left[\frac{\partial}{\partial\rho}(\varepsilon_r^c + \nu\varepsilon_t^c)\right](1-\rho^*) \qquad (3.31)$$

where ρ^* is the closest radial gauss point to $\rho=1$. Once the vector has been completed the nodal point values at $t=\Delta t$ can be obtained and the process repeated as many times as desired. In this manner, the code calculates the nodal point values as a function of time.

The integrating procedure used is the Adams-Bashforth predictor-corrector method [4]. Since the method is not self-starting, the fourth order Runge-Kutta method [4] is used for the first five time steps, and then the predictor-corrector algorithms (below) are used.

Predictor

$$\varepsilon_p^c(t+\Delta t)=\varepsilon^c(t)+\Delta t/24\Big[55\dot{\varepsilon}^c(\varepsilon^c(t))-59\dot{\varepsilon}^c(\varepsilon^c(t-\Delta t))$$

$$+37\dot{\varepsilon}^c(\varepsilon^c(t-2\Delta t))-9\dot{\varepsilon}^c(\varepsilon^c(t-3\Delta t))\Big] \qquad (3.32)$$

Corrector

$$\varepsilon_c^c(t+\Delta t)=\varepsilon^c(t)+\Delta t/24\Big[9\dot{\varepsilon}^c(\varepsilon_p^c(t+\Delta t))+19\dot{\varepsilon}^c(\varepsilon^c(t))+$$

$$-5\dot{\varepsilon}^c(\varepsilon^c(t-\Delta t))+\dot{\varepsilon}^c(\varepsilon^c(t-2\Delta t))\Big] \qquad (3.33)$$

The relative error, E, of integration can be estimated at each gauss point by the equation:

$$E=\left|\frac{\varepsilon_c^c-\varepsilon_p^c}{\varepsilon_c^c}\right| \qquad (3.34)$$

The relative error is used in the following way: if the largest error in the plate is less than 10^{-5}, then the step size Δt can be doubled without significantly hurting accuracy. Conversely, if the largest relative error is larger than 10^{-3}, the the step size will be halved and the integration redone.

In order to estimate the effect upon the results of neglecting the transverse shearing stress, the linear elastic result for the transverse shearing stress was included in the code. The elastic shear stress has the form [3]:

$$\tau_{rz}(\rho,\xi) = C_1(1-\xi^2)/\rho \tag{3.35}$$

where C_1 is a constant. C_1 can be determined by relating the shear force per unit length (equation (3.14)) to the average shear stress and by using the Mean Value theorem[7]. Thus:

$$Q = \frac{P}{2\pi R\rho} = \bar{\tau}_{rz}h = h/\rho\int_0^1 C_1(1-\xi^2)d\xi \tag{3.36}$$

where $\bar{\tau}_{rz}$ is the average shear stress throughout the thickness of the plate. Solving for C_1 yields:

$$C_1 = \frac{3P}{4\pi Rh} \tag{3.37}$$

so that $\tau_{rz}(\rho,\xi)$ becomes:

$$\tau_{rz}(\rho,\xi) = \frac{3P}{4\pi Rh\rho}(1-\xi^2) \tag{3.38}$$

Note that the shear stress calculated is assuming elastic conditions. However, given the fact that the actual shearing stress distribution must vanish at the top and bottom of the plate, must have a maximum at the center of the plate, and must satisfy the equilibrium equation (3.3), it seems likely that the actual distribution of transverse shearing stresses does not differ too greatly from the elastically calculated distribution. In order to estimate the influence of transverse shearing stresses upon the result, the finite element code was run to 10,000 hours a total of four times, using two differrent creep laws with or without consideration of transverse shear.

RESULTS

The exact elastic solution will be sought so that comparisions can be made with the finite element code's predictions at t=0, the initial experimental deflection, and the exact elastic solution. The solution is obtained from the governing differential equation for an elastic, symmetrically loaded circular plate[3]:

$$\frac{d}{dr}\left[\frac{1}{r}\frac{d}{dr}\left(r\frac{dw}{dr}\right)\right] = Q/D \qquad (4.1)$$

Nondimensionalizing the radius and substituting the expression for Q from equation (3.14) gives:

$$\frac{d}{d\rho}\left[\frac{1}{\rho}\frac{d}{d\rho}\left(\rho\frac{dw}{d\rho}\right)\right] = \frac{PR^2}{2\pi D} \qquad (4.2)$$

Integrating the above equation three times and enforcing the proper boundary conditions yields the plate deflection as a function of ρ.

$$w = \frac{PR^2}{16\pi D}\left[2\rho^2 \ln\rho + \left(\frac{3+\nu}{1+\nu}\right)(1-\rho^2)\right] \qquad (4.3)$$

Once the elastic deflection is known, the radial and tangential elastic strains can can be found by use of equations (3.1) and (3.2) and the stresses calculated by Hooke's law. In this way, the elastic radial and tangential stresses were found to be:

$$\sigma_{rr}(\sigma,\xi) = \frac{3P}{2\pi h^2}\,\xi \ln\rho \qquad (4.4)$$

$$\sigma_{tt}(\sigma,\xi) = \frac{3P}{2\pi h^2}\left[\,(1+\nu)\ln\rho + (1-\nu)\,\right] \qquad (4.5)$$

The polished beryllium disk tested at the Bureau of Standards had the following material constants and dimensions:

R=.025 m

h=.00325 m

$E=3.137 \times 10^{-6}$ MPa

ν=.08

$P=9.944 \times 10^{-6}$ MN

Using laser inferometry, the Bureau was able to measure the plate deflection to within 10^{-6} m. Comparisons between the elasticity solution, the predictions of the finite element code, and the experimental results are given in Table 2 below:

Table 2- Elastic Plate Deflection (μm)

ρ	Exact elastic	ρ	Finite element code	ρ	Experimental test
0.0	3.87	0.0	3.87	0.0	3.89
0.025	3.86	0.025	3.86	0.0244	3.86
0.05	3.84	0.05	3.84	0.146	3.67
0.1	3.77	0.1	3.77	0.268	3.35
0.2	3.54	0.2	3.54	0.390	2.89
0.4	2.85	0.4	2.85	0.512	2.40
0.6	1.98	0.6	1.98	0.634	1.80
0.8	1.00	0.8	1.00	0.756	1.20
1.0	0.0	1.0	0.0	0.878	0.60
				1.0	0.0

Note that the initial experimental deflection is in good agreement with the elastic solution.

The stresses in the finite element code were calculated at every gauss point and agreed to within three significant figure with the exact elastic stresses except at the first few radial gauss point near the center of the plate. The differences at ξ=.9036 (the gauss point closest to the plate surface) are shown in table 3.

Table 3- Elastic stresses at ξ=.9306 (MPa)

ρ	Exact elastic	Finite element code
.00282	σ_{rr}=26.5	σ_{rr}=27.16
	σ_{tt}=30.4	σ_{tt}=28.3
.0125	σ_{rr}=19.8	σ_{rr}=19.1
	σ_{tt}=23.6	σ_{tt}=23.8
.0222	σ_{rr}=17.2	σ_{rr}=16.9
	σ_{tt}=21.0	σ_{tt}=21.0
.0278	σ_{rr}=16.2	σ_{rr}=16.4
	σ_{tt}=20.0	σ_{tt}=20.0

The small differences in the predicted stresses near ρ=0 is probably due to the singular nature of the elastic stresses as ρ approaches zero. Given that the finite element code predicted the same deflections as the elastic solution to within three significant figures, and that the stresses are only slightly off near the origin, nine nodal points were deemed sufficient for creep analysis.

Starting from the elastic solution at t=0, the code was run to 10,000 hours using both of the creep law fits and also either including or excluding the effect of transverse shearing stresses. These predictions are compared with the experimental results in Table 4 and in Figure 3.

Table 4- Maximum Plate Deflection at t=10,000 hours (μm)

Fit #1 w/o Shear	Fit #1 w/ Shear	Fit #2 w/o Shear	Fit #2 w/ Shear	Experimental Deflection
4.00	3.99	4.28	4.27	4.24

Note that fit #2 produced fairly good agreement with the experimental results, while fit #1 does not. In addition, it can be seen that the inclusion of tranverse shearing stresses into the finite element code did not significantly affect the predictions of either curve fit.

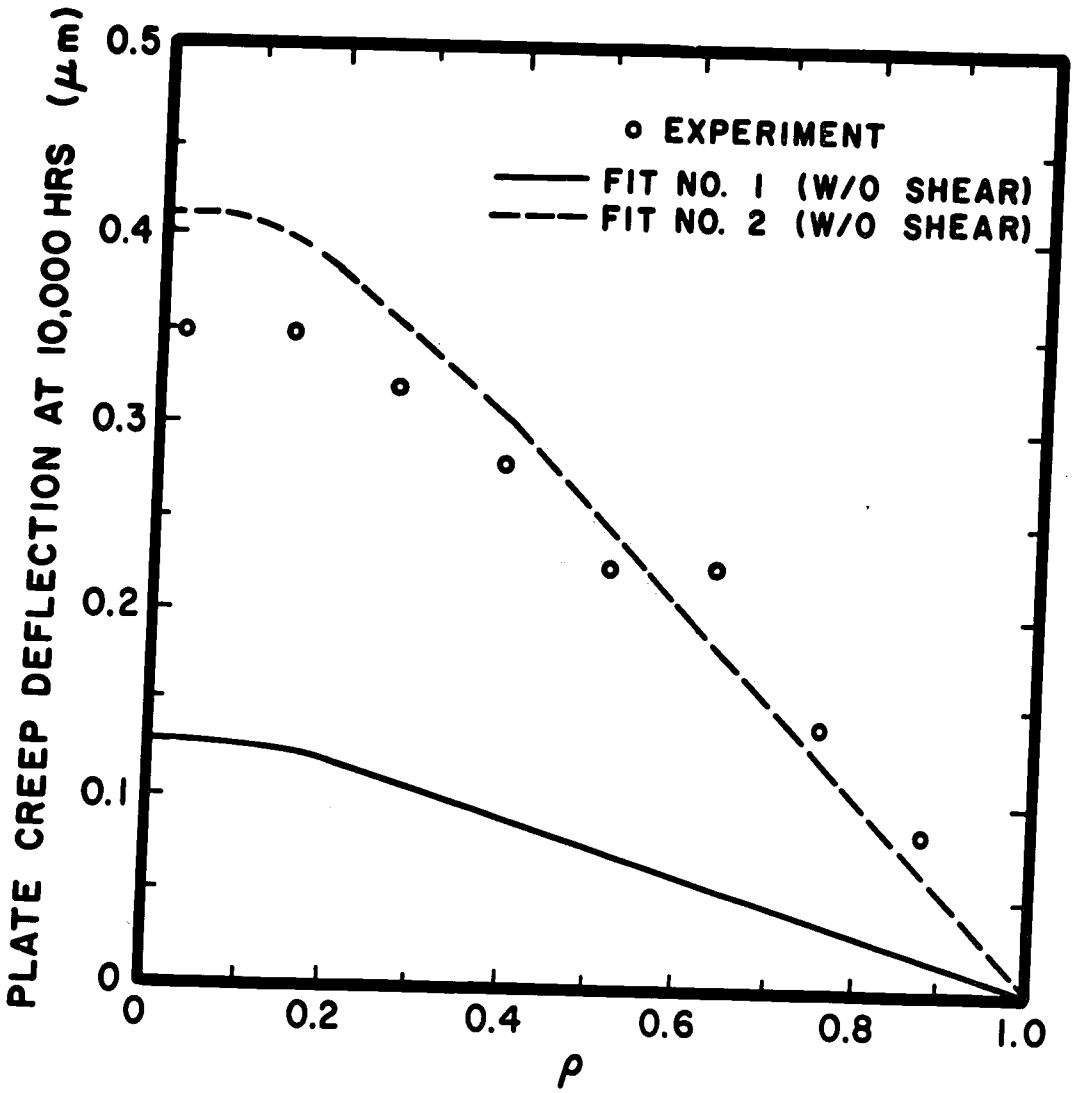
PLATE CREEP DEFLECTION AT 10,000 HRS (μm)
0.5
0.4
0.3
0.2
0.1
0
0
0.2
0.4
0.6
0.8
1.0
ρ
o EXPERIMENT
FIT NO. 1 (W/O SHEAR)
FIT NO. 2 (W/O SHEAR)

Fig. 3.

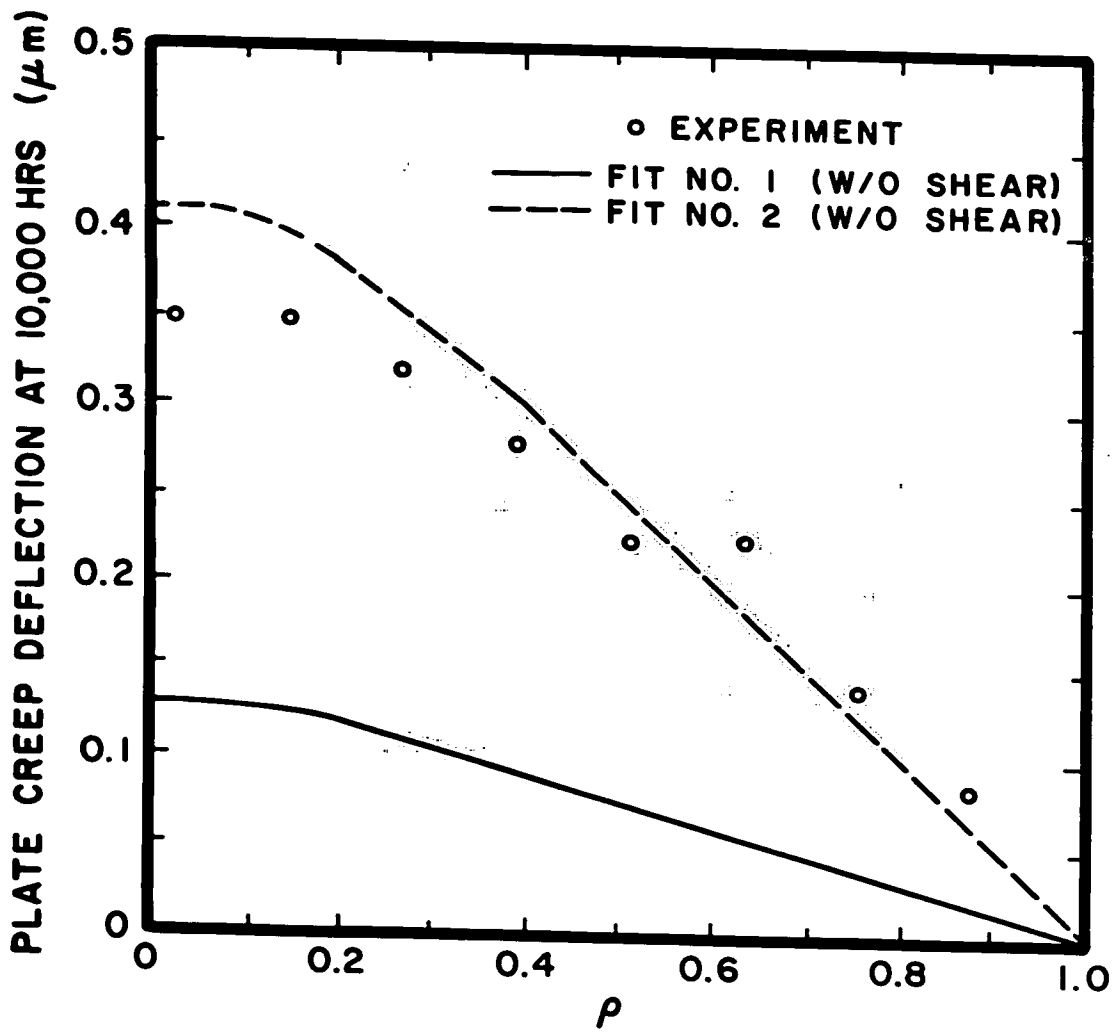
PLATE CREEP DEFLECTION AT 10,000 HRS (μm)
0.5
0.4
0.3
0.2
0.1
0
0
0.2
0.4
0.6
0.8
1.0
ρ
o EXPERIMENT
FIT NO. 1 (W/O SHEAR)
FIT NO. 2 (W/O SHEAR)

Fig. 3.

CONCLUSIONS

The results given in Table 4 show that the experimental maximum deflection lies between those predicted by fits #1 and #2, though fit #2 shows much better agreement than fit #1. Given the scarcity of available data and the wide divergence between the results of the two tests conducted at 69.0 MPa, it is not surprising that the two predictions differ by so much, since the multiaxial law is directly derived from the uniaxial data. However, because the experimental deflection at 10,000 hours lies between the finite element code's predictions using the two different fits, and is reasonably close to the results obtained using fit #2, it is felt that the inaccuracies encountered are due to the limited data available to develop the multiaxial creep law, and not to the code itself. The inclusion of transverse shearing stresses into the multiaxial creep law was found to have a negligible effect on the predictions of either fit.

This investigation has shown the difficulty in precisely predicting multiaxial microcreep in beryllium subject to a spatially varying stress state. Scatter in creep data is rather common, hence any predictions of creep under multiaxial conditions are subject to a certain amount of error. With this in mind, reasonably accurate predictions of multiaxial tests are possible, but precision to the same degree seen in elastic tests cannot be expected.

APPENDIX

$\phi(\rho)$ is approximated with C^1 hermitian interpolating functions by the sum [6]:

$$\phi(\rho) = N_0(\rho)\phi_0 + N_1(\rho)\phi'_0 + N_2(\rho)\phi_1 + N_3(\rho)\phi'_1 + \ldots$$

$$\ldots + N_{2n-2}(\rho)\phi_n + N_{2n-1}(\rho)\phi'_n$$

By defining:

$$h = \rho_{i+1} - \rho_i$$

and $s = (\rho - \rho_i)/h$

where ρ_i and ρ_{i+1} are the values of ρ at the nodal points i and i+1 respectively, the C^1 interpolating functions can be written:

$$N_0(\rho) = \begin{cases} (s-1)^2(1+2s) & \rho_0 < \rho < \rho_1 \\ 0 & \rho > \rho_1 \end{cases}$$

$$N_1(\rho) = \begin{cases} hs(s-1)^2 & \rho_0 < \rho < \rho_1 \\ 0 & \rho > \rho_1 \end{cases}$$

for $j=1,2,\ldots,n-2$

$$N_{2j}(\rho) = \begin{cases} s^2(3-2s) & \rho_{i-1} < \rho < \rho_i \\ (s-1)^2(1+2s) & \rho_i < \rho < \rho_{i+1} \\ 0 & \text{elsewhere} \end{cases}$$

$$N_{2j+1}(\rho) = \begin{cases} hs^2(s-1) & \rho_{i-1} < \rho < \rho_i \\ hs(s-1)^2 & \rho_i < \rho < \rho_{i+1} \\ 0 & \text{elsewhere} \end{cases}$$

$$N_{2n-2}(\rho) = \begin{cases} s^2(3-2s) & \rho_{n-1} < \rho < \rho_n \\ 0 & \rho < \rho_{n-1} \end{cases}$$

$$N_{2n-1}(\rho) = \begin{cases} hs^2(s-1) & \rho_{n-1} < \rho < \rho_n \\ 0 & \rho < \rho_{n-1} \end{cases}$$

REFERENCES

[1] Polvani, R.S., Christ, B.W., and Fuller, E.R., Beryllium Micro-Deformation Mechanisms , Creep and Fracture of Engineering Materials and Structures, University College, Swansea, U.K., 1981.

[2] Kraus, H., Creep Analysis, John Wiley and Sons, New York, 1980.

[3] Timoshenko, S., and Woinowsky-Krieger, S., Theory of Plates and Shells, Second Edition, McGraw-Hill, New York, 1959.

[4] Gerald, C.F., Applied Numerical Analysis, Addison-Wesley, Reading, Massachusetts, 1979.

[5] Garofalo, F., Fundamentals of Creep and Creep Rupture in Metals, MacMillan, New York, 1965.

[6] Huebner, K.H., and Thornton, E.A., The Finite Element Method for Engineers, Second Edition, John Wiley and Sons, New York, 1982.

[7] Shenk, A. Calculus and Analytical Geometry, Goodyear, Santa Monica, California, 1979.

VITA

The author was born on June 27, 1961 to Louis E. and Dorothy H. Povirk in Pittsburgh, Pennsylvania. He attended public schools in McCandless, Pa., and graduated from North Allegheny High School in June, 1979 with honors.

He entered Lehigh University in September, 1979 and was awarded the degree of Bachelor of Science in Mechanical Engineering in June, 1983. He is a member of Tau Beta Pi and Pi Tau Sigma engineering honor societies.

He began graduate study at Lehigh in September, 1983 and expects to be awarded the degree of Master of Science in Mechanical Engineering in January, 1985.